PHILOSOPHICAL TRANSACTIONS A

Phil. Trans. R. Soc. A.
doi:10.1098/not yet assigned

Identifying the ingredients of hydrous arc magmas: insights from Mt Lamington, Papua New Guinea

Humphreys, M.C.S., Zhang, J., Cooper, G.F., Macpherson, C.G. & Ottley, C.J.

Department of Earth Sciences, Durham University, Science Labs, Durham, DH1 3LE, UK

Keywords: Mt Lamington, subduction, magma, crystal textures, amphibole, trace elements

Summary

Volcanism is the surface expression of magma intrusion, crystallisation, assimilation and hybridisation processes operating throughout the crust over a range of time periods. Many magmas, including those erupted at subduction zones, have complex textures that reflect these processes. Here we use textural and geochemical characteristics of calcic amphiboles to help identify multiple ingredients of subduction zone magmatism at Mt Lamington volcano, Papua New Guinea. Our approach utilises existing trace element partitioning schemes to calculate the compositions of amphibole equilibrium melts (AEM). The AEM compositions show that Mt Lamington andesites and plutonic enclaves are dominated by fractionation of amphibole + plagioclase + biotite, with assimilation of plagioclase and zircon. Magnesiohastingsite crystals in the andesite and diktytaxitic mafic enclaves reflect multiple episodes of recharge by more primitive, geochemically variable melts. The andesite also contains clots with rounded grains and melt on grain boundaries. These features indicate slow crystallisation, and the retention of melt films could significantly enhance the potential for remobilisation of crystals by infiltrating melts or during magma mixing. Variations in crystallisation conditions could thus significantly affect the mush microstructure. We suggest that this could result in significant bias of the volcanic record towards the preferential incorporation of more slowly cooled plutonic material from the lower crust or from more thermally mature plumbing systems.

Introduction

The ability to interpret the crustal-scale structure of magmatic plumbing systems beneath active volcanoes is of great interest because it may help us to understand eruptive activity at the surface. Understanding the nature of the magmatic plumbing system could aid the interpretation of surface gas emissions and other precursory volcanic activity. The whole-rock composition of samples erupted at the surface can bear fundamental clues to the origins of magmatism and nature of melting conditions. However, the textures and compositions of crystals are often complex, as a result of interactions and processes happening during different stages of growth [1]. Whole-rock compositions therefore represent a time-integrated average of different processes, commonly including multiple episodes of magma mixing [2-6]. It is therefore critical to understand the significance of variations in mineral textures and geochemistry, in order to see through any whole-rock averaging processes and gain insights into the details of the processes operating in different parts of the volcanic plumbing system.

Mineral and melt studies are important in defining the potential range of pressures and temperatures of magma generation and storage, as well as the chemical composition of host melts. The trace element compositions of minerals are derived from the characteristics of their host melts, which means that knowledge

*Author for correspondence (madeleine.humphreys@durham.ac.uk).
†Present address:
Department, Institution, Address, City, Code, Country

of crystal-melt partitioning can be used to reconstruct the chemistry of the parental melt during crystallisation. Here we focus on subduction (arc) settings, where magmas are particularly rich in dissolved volatiles. Here, amphiboles can be used to examine diverse host melt compositions, because they are a common constituent of subduction zone magmas, are stable across a wide range of pressure, temperature and melt composition, and incorporate essential volatiles. Unlike many other minerals, the mineral structure of amphiboles contains four different cation sites of different shapes and sizes, which can incorporate an array of trace elements with different charge, radius and electronegativity. The trace element signatures of amphiboles can therefore be used to give a new depth of information about the range of processes operating underneath active subduction zone volcanoes. Here we discuss the causes of variable amphibole geochemistry in magmas erupted at Mt Lamington, Papua New Guinea, combining textural observations with novel geochemical interpretations based on a recent amphibole-melt trace element partitioning scheme. We show that the system records a long history of mixing of chemically variable, small-volume basaltic-andesite to andesite melts, interacting with more evolved magmas undergoing *in situ* differentiation. We also show that the textures of intrusive mushy materials, found incorporated in the eruptive products as small inclusions, are critical in determining their tendency to be remobilised and assimilated by later pulses of magma. This suggests that volcanic products may show a systematic bias towards preferential remobilisation of slowly cooled plutonic material and thermally mature volcanic systems, over more rapidly cooled materials or thermally immature systems.

MAGMATIC CRYSTAL TEXTURES

Igneous rock textures typically include four categories of crystals [7]: (i) phenocrysts – crystals that grew directly from the magmatic system; (ii) antecrysts – crystals derived from the magmatic system (*sensu lato*; see [8]); (iii) xenocrysts – foreign crystals derived from external sources; and (iv) microlites – small grains growing directly from the late-stage melt, immediately prior to or during eruption. When using crystal chemistry and textures to interpret magmatic processes, it is essential to consider the extent of local equilibration at every step; this changes as a function of spatial lengthscale and equilibration time [9]. However, it has been recognised that in many systems, magmas probably reside in a largely mushy state for significant parts of their lifetime [e.g. 10-13], and that magma assembly involves late-stage reorganisation and juxtaposition of components from different sources prior to eruption [e.g. 4, 14-18]. In many intermediate (andesite to dacite) magmas, it is hard to classify crystals as either 'antecrysts' or 'phenocrysts' because they incorporate multiple stages of crystallisation, resorption and regrowth under conditions that may be variably out of equilibrium with the carrier liquid. Thus they represent materials that have experienced numerous transitions between different physical (mush or melt-rich, variable temperature and pressure) and chemical (varying melt composition) environments over extended periods of time and space within the magmatic system (e.g. [19]). The crystal zoning therefore represents a capsule of information about the variability in P-T-X conditions that can help us to understand the physical architecture of the magmatic plumbing system.

GEOLOGICAL BACKGROUND

Mt Lamington is an active, dome-forming andesitic volcano located on the southeastern Papuan peninsula, where volcanic activity has occurred since the middle Miocene [20]. There are three other Quaternary edifices in the region, including Mt Victory, Mt Trafalgar and Hydrographers Range (see figure 1 of [21] and references therein). Mt Lamington has only three confirmed Holocene eruptions; the most recent was a Peléean style eruption that began in 1951 with a large explosion and was followed by persistent dome growth [22]. The tectonic setting of the wider region is complex, with the locus of volcanism apparently decoupled from regions of active subduction, as the Trobriand Trough to the north lacks a seismically defined Benioff Zone [23,24]. Johnson et al. (1978) [25] suggested that the present activity may be a result of decompression melting of previously subduction-modified mantle. Mt Lamington overlies a thick sequence of ophiolite material known as the Papuan Ultramafic Belt (PUB, [26,27]), which has been interpreted as a source of the high Ni and Cr concentrations of whole-rocks [23].

Previous studies have described the whole-rock geochemistry and petrology of eruptive products from Mt Lamington, focusing on the origin of Ni and Cr enrichment and the source of sulphate [23], and on defining the variations in mineral chemistry and constraining the formation of the 1951 andesite [21]. Arculus et al. (1983) [23] attributed the broad geochemical variations seen in the amphiboles to interactions with, and contamination by, partially melted ophiolite material from the PUB. The andesites contain partially equilibrated olivines (Fo_{85}) in varying stages of reaction with the host melt, identified by the crystallisation of

rims of orthopyroxene + oxide, then amphibole [21,23]. However, these olivine compositions are dissimilar to olivine in xenoliths of the harzburgite and dunite, and the PUB basalts are reported to be rarely olivine-phyric, so the olivines are thought not to derive from the PUB [21]. Instead they are attributed to assimilation of the products of older, more primitive magmas within the Mt Lamington volcanic plumbing system, together with rare clinopyroxene xenocrysts [21]. This finding prompted us to reassess the causes of amphibole geochemical zoning at Mt Lamington, using new trace element data and partitioning methods to reconstruct both major and trace element compositions of the equilibrium melts. The samples studied are those of [21] and [23] and include andesite lavas, diktytaxitic enclaves and plutonic-textured enclaves collected from the crater area or northern-facing slopes of the 1951 eruption. As described in [21] the andesites are porphyritic with ≥50% crystallinity dominated by plagioclase and amphibole with minor biotite, Fe-Ti oxides and pyroxenes, together with xenocrystic olivine. Accessory minerals are apatite + zircon ± anhydrite. The groundmass is variably devitrified, with microlites of plagioclase and oxide and small crystals of amphibole and biotite that may be fragments of larger grains. The diktytaxitic enclaves are vesicular with abundant, elongate crystals and glassy matrix. Plutonic-textured enclaves are coarser grained, with low vesicle content and high overall crystallinity.

Methods

Electron microprobe analyses of amphiboles were carried out at Edinburgh University, using a Cameca SX-100 electron microprobe equipped with five wavelength-dispersive spectrometers. Amphiboles were analysed using a 15 kV accelerating voltage, with 10 nA beam current for major elements and 100 nA for trace elements, and a 10 µm defocused beam. Matrix corrections were conducted using a PAP correction procedure. Calibration standards were wollastonite (for Si, Ca), spinel (Al, Mg), fayalite (Fe), jadeite (Na), orthoclase (K), rutile (Ti), celestite (Sr), pure metal (Mn), NaCl (Cl) and synthetic $RbMnF_3$ (F). Secondary standards included St John's Island olivine, USGS glass BCR-2G and Lipari obsidian. The dataset builds on that reported by [21].

Trace element concentrations of amphiboles were analysed by laser ablation-inductively coupled plasma-mass spectrometry (LA-ICP-MS) at Durham Geochemistry Centre, Durham University. A NewWave UP193 laser ablation system was coupled to a Thermo Scientific X-Series 2 quadrupole mass spectrometer. The analyses were carried out on standard polished thin sections after removal of surficial carbon coat. Amphiboles were analysed using a 75 µm laser beam, with a 5 Hz repetition rate, 80% power conditions and output energy of ~ 6.0 mJ. The instrument was optimized to give high sensitivity across the analysed mass range, with low levels of oxide formation, assessed using the ratio U/Th. Each spot was ablated for 60 s (dwell time) with 60 s of washout between ablations. The ablated particles were transported into ICP-MS using a He-Ar carrier gas. NIST-612 was used as the calibration standard and was analysed at the beginning, in the middle and at the end of each run. NIST610, BHVO-2G and BCR-2G were used as secondary standards to monitor and correct for instrumental drift. Data were reduced and processed using Iolite software [28,29] using Ca as the internal standard.

Trace element amphibole-melt partition coefficients were calculated using the relationships given by [30], which were based on a multiple regression analysis of 145 published experimental measurements of partition coefficients from 13 studies. A summary of the method is given in the supplementary information. The regression data included melt compositions from basanite to rhyolite, and P-T conditions from 200-2500 MPa and 780-1100 °C. The amphiboles crystallised from the experimental studies were calcic amphiboles in the range pargasite – edenite – hastingsite – magnesiohastingsite (MgHst) – tschermakite (Tsch) – magnesiohornblende (MgHbl). The analysis takes into account the effect of the major element composition of the amphibole on the trace element partitioning, using amphibole formula components calculated on the basis of 23 oxygens and using the "average Fe^{3+}" scheme of [31]. The calculations are independent of pressure and temperature. Having calculated partition coefficients, we used the measured trace element composition of each amphibole analysis to calculate the trace element concentrations of its equilibrium melt. The equivalent major element compositions of the equilibrium melts were calculated using [21; Zhang et al. erratum].

Results

Andesites from Mt Lamington contain ~18-26 vol% amphibole, whereas mafic enclaves with diktytaxitic texture contain ~40-47 vol% amphibole, as summarised by [21,23]. Exchange of crystals between the andesite and mafic enclaves is common, as inferred by overlap of textures and mineral chemistry [21]. Elongate

(framework-forming) grains in mafic enclaves have high Ti, Al_{tot}, Mg# and Al contents (typically 10-13 wt% Al_2O_3) and low FeO and MnO (Figure 1). Outer rims of framework-forming grains and large crystals inherited from the andesite record lower Al contents (9-11 wt% Al_2O_3; [21]). Here we will present only data from the framework-forming grains as belonging to the diktytaxitic enclaves (i.e. ignoring inherited crystals); these grains are largely MgHst. The andesite contains MgHbl-edenite phenocrysts that are typically more Al-poor, in the range 7.5-10 wt% Al_2O_3, with higher MnO and FeO and lower Mg# and Al_{tot} (figure 1). A minority of analyses overlapping with the MgHst amphiboles in the diktytaxitic enclaves are interpreted as inherited crystals based on geochemistry and textures [21]. Amphiboles from plutonic-textured enclaves have intermediate Al contents, typically in the range ~8.5-10.5 wt% Al_2O_3 and intermediate MnO and FeO (Figure 1; supplementary table 1). These crystals are also classified as MgHbl-edenite-MgHst and overlap in Mg#-Al_{tot} space with amphiboles from the andesite (figure 1). Amphiboles from rare trachybasalts, also erupted from Mt Lamington, were analysed by [23] and [21] and are K-rich MgHst with >3 wt% TiO_2, and are distinct from anything observed in the andesites or their inclusions (Figure 1).

Amphibole trace element concentrations reflect the variations in major element composition. The low-Al amphiboles from the andesite typically contain 60-200 ppm Sr, 30-70 ppm Zr, 5-10 ppm Nb, 10-22 ppm La, and 4-8 ppm Yb (Supplementary data table). High-Al amphiboles from the diktytaxitic enclaves typically contain higher concentrations of Sr (300-450 ppm) and Zr (50-70 ppm), with lower concentrations of Nb (2-6 ppm), La (3-10 ppm), and Yb (1-5 ppm) (Supplementary data table). Trace element concentrations of amphiboles from the plutonic-textured enclaves fall within the andesite range: 75-150 ppm Sr, 40-60 ppm Zr, 3-6 ppm Nb, 10-15 ppm La and 3-5 ppm Yb. The cores of some grains have anomalously high Cr contents (as determined by EPMA, [21, 23]).

Using the trace element partitioning schemes of [30] and the major element regression scheme of [32; Zhang et al. erratum] we calculated the compositions of melts in equilibrium with the amphiboles ('amphibole equilibrium melts', AEM). Low-Al amphiboles from the andesite give AEM with 69-77 wt% SiO_2 (average 73 wt% SiO_2, $n = 74$) and 0.2-0.7 wt% MgO, with the few Mg-Hst crystals giving 57-71 wt% SiO_2 and 0.6-3.5 wt% MgO ($n = 22$; Supplementary data table). Amphiboles from plutonic-textured enclaves yield AEM that overlap strongly with these compositions. AEM from the diktytaxitic enclave high-Al amphiboles are distinctive, with lower SiO_2 (56-69 wt%) and higher MgO (0.6-4.1 wt%) and CaO (2.7-7.2 wt%). The lower Al_2O_3 contents of some of the crystal rims gives a range of AEM that approaches those from the andesite.

For trace elements (Figures 2-3), we predict that AEM for the andesite have typically 35-130 ppm Zr, 3-8 ppm Nb, 180-550 ppm Sr, 15-35 ppm La and 0.6-1.8 ppm Yb. La/Yb values are in the range 10-30, Sr/Y typically 7-25, and Eu/Eu* 0.9-1.2. Chondrite-normalised rare earth element (REE) profiles have a slightly concave-upward shape, with slightly higher LREE/HREE values than the whole rocks (data from [21]), and lower MREEs (figure 4). Plutonic amphiboles yield AEM with similar trace element compositions to the andesite low-Al amphiboles, but with slightly lower Y, Sm (1.5-2.5 ppm) and Yb (0.6-1.4 ppm), resulting in higher Sr/Y and La/Yb. Chondrite-normalised rare earth element profiles have a clear concave-upward shape, with a minimum near Dy (figure 4). High-Al amphiboles from the diktytaxitic enclaves return AEM with a much broader range of trace element concentrations, from 100-230 ppm Zr, 7-17 ppm Nb, 400-1000 ppm Sr, 20-60 ppm La and 1-3 ppm Yb (Figure 2). La/Yb values are in the range 10-24, Sr/Y from 35-55 and Eu/Eu* 1.0-1.3 (Figure 3).

Zhang et al. (2015) [21] recognised two kinds of 'oscillatory zoned' amphiboles (i.e, those showing multiple excursions to higher Mg#) in the andesite, with 'spiky' and 'diffuse' zonation patterns (supplementary figure 1). Spiky zoned crystals have multiple abrupt core-rim zones, from MgHbl-edenite to low-Mg# MgHst, while diffuse-zoned crystals have one or two broad zones with gradational boundaries, from MgHbl-edenite to high-Mg# MgHst. The distinction is defined at Mg# = 0.70, where there is natural break between the two populations (supplementary data table). The two populations differ in their trace element concentrations, with the diffuse-zoned crystals showing generally higher HFS (Zr, Nb) and rare earth element concentrations than spiky-zoned grains. This translates into significant differences in predicted major and trace element AEM compositions, with the diffuse-zoned crystals showing lower Sm/Yb and higher Zr, Nb and Sr at a small range in SiO_2 (57-69 wt%), compared with spiky-zoned grains (65-71 wt% SiO_2) (Figures 2,3).

Plagioclase is present in the andesites, plutonic enclaves and diktytaxitic enclaves, covering a wide range of compositions from An_{95}-An_{30} in each rock type [summarised by 21]. These data show that plagioclase microphenocryst cores from the diktytaxitic enclaves generally have higher Sr concentrations (2500-3100 ppm), compared to their rims (1750-2800 ppm). Plagioclase from the plutonic-textured enclaves have 2100-3100 ppm Sr, while Sr contents of plagioclase from the andesite are more strongly heterogeneous (1780-3100 ppm in rim analyses; average ~ 2300 ppm). The differences in minor and trace element concentrations are

interpreted to reflect variations in melt composition, and these are most clearly evident when plotting FeO/K$_2$O vs Sr (Figure 5), where sieved plagioclase rims from the andesite and plagioclase microphenocrysts from the diktytaxitic enclaves trend strongly towards higher FeO/K$_2$O. We used the partition coefficients of [33] to calculate equilibrium melt Sr concentrations from the plagioclases, for comparison with AEM compositions. The cores of microphenocrysts from the diktytaxitic enclave (calculated at 960 °C based on amphibole-plagioclase thermometry, [21]) give equilibrium melts with 570-840 ppm Sr, and the rim compositions return melts with 290-640 ppm Sr. These values agree well with Sr contents of AEM for the diktytaxitic enclave (Figure 2). For the andesite and plutonic enclave, amphibole-plagioclase thermometry indicates average temperatures of ~ 850 °C [20] and this agrees well with temperatures inferred from the amphiboles alone (see figure 1, following [34]). At 850 °C, calculated equilibrium melts for plagioclase from both the andesite and the plutonic enclave have a wide range of Sr concentrations: 270-840 ppm Sr for the andesite (calculated at 850 °C based on amphibole-plagioclase thermometry, [20]), and 300-900 ppm Sr for the plutonic enclave (also calculated at 850 °C). This could be related to the presence of relatively primitive cores from earlier in the evolution of the magma (see discussion below).

Discussion

A long history of mixing with geochemically variable melts

The major element compositions of AEM from the diktytaxitic enclaves show that the magmatic system at Mt Lamington contains (or has contained) packets of melt that are significantly less evolved than the matrix of the erupted andesites, extending to basaltic-andesites with ~55 wt% SiO$_2$. Although the SiO$_2$ contents of these melts are similar to the whole-rock compositions of the mafic enclaves, their predicted trace element concentrations typically do not agree well with the mafic enclave whole-rock compositions. This can be explained given that the enclave whole-rocks contain crystals of olivine + spinel ± clinopyroxene ± amphibole that are hypothesised to be derived from deep cumulates [21], plus mechanically incorporated phenocrysts of plagioclase and amphibole mixed in from the andesite. In contrast, equilibrium melt compositions calculated from plagioclase (excluding the most evolved rims) from the diktytaxitic enclaves and sieved crystals in the andesite have Sr contents of 560-975 ppm, and these agree well with Sr contents of AEM from framework-forming amphiboles in the diktytaxitic enclaves. The consistency between different estimates of melt composition supports our use of the calculated AEM to represent the diversity of melt compositions.

The AEM from the diktytaxitic enclaves show strong trace element variations with increasing SiO$_2$ and other major element indices of melt evolution. Some incompatible elements (such as Pb) are enriched with increasing SiO$_2$. Sr decreases with increasing SiO$_2$ (Figure 2), as would be expected for melts that are crystallising plagioclase (Figure 2). However, if these geochemical variations are ascribed to fractional crystallisation, then the strong decreases in elements such as Zr and Nb would require fractionation of accessory minerals including zircon and ilmenite. Even though these phases are stable in the andesite whole rocks (which have a rhyolitic matrix glass), it is hard to accept that zircon is fractionating from a basaltic andesite melt with only 150 ppm Zr (following [35]). An alternative is that the chemical trends in the AEM are the result of mixing between enclave-forming magma(s) and a putative dacite melt with approximately 68 wt% SiO$_2$. This composition is based on the location of the break in slope in plots of La/Yb or Sm/Yb vs SiO$_2$ or Sr (Figure 3). The break in slope in Sm/Yb suggests a change in magmatic processes from mixing (resulting in decreasing Sm/Yb) to amphibole fractionation (resulting in increasing Sm/Yb). The composition of the putative dacite, at ~68 wt% SiO$_2$, is similar to the least evolved AEM predicted from amphiboles in the andesite and/or plutonic enclaves (see *The formation of andesite and cumulate-textured enclaves at Mt Lamington*, below).

The diffuse-zoned high-Mg# MgHst and spiky-zoned low-Mg# MgHst amphiboles, which are both found in the andesite, represent a record of crystallisation during excursions to more primitive and/or hotter melts that are not seen in the eruptive record. This can also be seen in Mg#-AlIV relationships (figure 1; [34]). This is distinct from the episode of mixing with the observed diktytaxitic enclave magma, which results in sharp compositional zones on the rims of amphibole phenocrysts inherited from the andesite, recording an event that took place shortly before eruption. The overall suite of amphibole trace element data therefore preserves information about the longer-term record of variable melt compositions and physical conditions in the magmatic storage system, with multiple instances of interactions with more primitive melts. The somewhat gradational nature of the diffuse amphibole zoning implies that significant amounts of time were available for partial diffusive equilibration of Fe and Mg after the mingling event(s), though not long enough for slower-diffusing elements to experience modification (zoning remains sharp for Al, Ti and Na, [21]). We emphasise

that any diffusive equilibration in the amphiboles themselves has a relatively limited effect on calculated AEM (less than the primary regression uncertainty, based on an analysis of smoothly zoned regions of the diffusely-zoned geochemical profiles). This is because re-equilibration primarily involves Fe-Mg interdiffusion and does not involve changes in other more slowly diffusing elements.

While both the diffuse-zoned MgHst and amphiboles from the diktytaxitic enclaves attest to crystallisation from more primitive melts, they have variable AEM trace element signatures, suggesting subtle temporal variations in the primitive melt compositions under Mt Lamington. AEM from the diffuse-zoned and diktytaxitic amphiboles overlap for most elements, but AEM from the diffuse-zoned amphiboles tend to have distinctly lower Nb concentrations, and thus lower Nb/La, than the diktytaxitic amphiboles (Figures 2, 3). Both AEM populations also show significant variance in absolute trace element concentrations, which decreases with increasing SiO$_2$ (Figures 2, 3). We suggest that this reflects real variability in trace element composition of small parcels of melt within the plumbing system, which is gradually eliminated during mixing ± crystallisation, as observed in other settings such as Iceland [36] and New Zealand [37]. Conversely, the abrupt nature of the spiky zonation indicates more recent mixing events with little time available for diffusive modification of the resulting zoning profiles. AEM from spiky-zoned MgHst tend to have higher REEs and Pb, and lower Sr and Sm/Yb (Figures 2, 3) and their compositions are more SiO$_2$-rich, closer to AEM from the andesite MgHbl, and typically distinct from AEMs from the diktytaxitic enclave and diffusely-zoned amphiboles. The variance in inferred trace element compositions is large, again suggesting significant melt variability within the system for the more recent mixing events.

The formation of andesite and cumulate-textured enclaves at Mt Lamington

The origin of the putative dacite melt, inferred from the break in slope of geochemical variations, is ambiguous. The ratio Sm/Yb is relatively low (figure 3), which could be consistent with the presence of amphibole in the melt source. One scenario for the formation of the dacite is peritectic melting of amphibolite [38] and subsequent ascent of the resulting melt from the lower crust until it stalls in a shallow magma storage region. The putative dacite melt at Mt Lamington has similar major element composition to the more evolved glasses produced experimentally from the cpx + melt = hbl peritectic reaction at high initial H$_2$O content [38], lending support to this hypothesis. However, it is difficult to distinguish this from the alternative case of prior amphibole fractionation from a less evolved precursor melt. Amphibole fractionation would drive the residual melt to higher SiO$_2$, lower Dy/Yb and higher La/Yb, as seen in many arc whole-rock suites [39], and to lower Nb/Ta [40]. Fractionation of amphibole at depth is also consistent with the presence of amphibole as a common phase in plutonic and cumulate nodules in arc lavas [41-44]. The strongly zoned cores of some amphiboles (spiky and diffuse MgHst zoning as described above) indicate the presence of more primitive (andesite to basaltic andesite) melts in the system, but do not clearly define any kind of fractionation trend. Sr and Nd isotopic compositions of the andesites and plutonic and diktytaxitic enclaves overlap [21] which indicates that localised partial melting of the crust by ascending mafic melts is not significant.

The AEM from the andesites have a predicted average Eu/Eu* (calculated as Eu/√(Sm$_n$*Gd$_n$) where N denotes chondrite-normalised to the values of Taylor & Maclennan 1980) of ~0.9, with a large range from ~1.2 to ~0.7, decreasing with increasing SiO$_2$. This compares with average values of ~1.0 for AEMs from the plutonic enclave (Figure 3). The highest values for any analysis are seen at ~68 wt% SiO$_2$. AEMs from the diktytaxitic enclave and from zoned MgHst crystals have Eu/Eu* slightly higher than those of the andesite, but are similarly variable (from ~0.8 to ~1.4), increasing with increasing SiO$_2$ (Figure 3). While the uncertainties on these values are large, the positive Eu anomaly seen in AEM from zoned MgHst, diktytaxitic amphiboles and some amphiboles from the andesite could realistically be generated by (i) fractionation of amphibole, which leaves a residual melt enriched in Eu, or (ii) remelting of plagioclase-bearing cumulates [45-46]. Taken together with the discussion above, we suggest that the putative dacite melt at Mt Lamington is derived by deep fractionation of amphibole from a relatively low-SiO$_2$ precursor melt. In contrast, the decreasing Eu/Eu* in the andesites is consistent with *in situ* fractionation involving plagioclase.

AEMs from the plutonic-textured enclave AEMs show increasing La/Yb, increasing Sm/Yb and constant (but scattered) Dy/Yb with increasing SiO$_2$. The AEMs show clear decreases in absolute abundance of Sr, Ti and all REE, and scattered decreases in Nb and Zr. This is consistent with *in situ* fractional crystallisation of an assemblage of amphibole + plagioclase + Fe-Ti oxide + biotite ± zircon ± apatite, as observed in the enclaves. Whereas AEM from the diktytaxitic amphiboles are similar to the diktytaxitic enclaves in major element composition, the plutonic-textured enclaves have whole-rock compositions that are less evolved than their AEM by at least ~10 wt% SiO$_2$ (see Figure 2). The discrepancy between AEM and the whole-rock compositions suggests either extraction of melt or the accumulation of solid phases in the whole-rocks. The plutonic

enclaves contain large clusters of amphibole + biotite, sometimes with a core rich in small oxide inclusions (Figure 7a). Following [21] we suggest that this is related to the complete reaction of olivine, derived from more primitive magmas that have completely reacted with matrix melt. This is consistent with the high Cr contents of some amphibole and clinopyroxene cores and also explains the enrichment in Ni, Cr and V in the plutonic enclave whole-rocks [21, 23].

Differences in rare earth element ratios and high field strength element abundances confirm that the andesite whole-rocks and the plutonic enclaves are likely not related by fractional crystallisation (see Figures 2,3). The AEM from the andesites are more scattered than those of the plutonic enclave, but they show some of the same trends with SiO_2 as the plutonic enclave AEM. This suggests that the andesites evolve by a similar process to the plutonic enclaves, i.e., *in situ* fractional crystallisation of plagioclase + amphibole + Fe-Ti oxide + biotite + zircon + apatite. This process is interrupted by intervals of mingling with the more mafic melts, as demonstrated by the presence of zoned crystals and inherited grains. The andesite whole-rocks are enriched in both Zr and Sr compared with the AEM. This suggests that the whole-rocks are also carrying a crystal cargo that includes both plagioclase and zircon. The andesite whole-rocks have a slightly negative Eu anomaly (Figure 3) but this may reflect a combination of plagioclase fractionation and assimilation.

Solidification, remobilisation and the generation of intermediate magmas

Textural observations coupled to AEM data clearly highlight that interactions between melt-rich magmas are common at Mt Lamington, as with other intermediate arc volcanoes. However, the comparison of whole-rock trace element compositions with AEMs indicates assimilation or remobilisation of a solid crystal cargo including plagioclase and zircon. To date there is no study of zircon textures from Mt Lamington but the andesites contain large individual or glomerocrystic plagioclase with complex patchy zoned and strongly oscillatory zoned cores (e.g. figure 2 of [21]). Complete reaction and assimilation of olivine crystals is shown by the presence of coarse clots of amphibole + biotite ± oxides (figure 7a and [21]). Disaggregated plutonic-textured material is also found in the andesites and diktytaxitic enclaves (Figure 7d). Taken together, this textural evidence suggests that mechanical remobilisation is a relatively common process. However, the exact mechanism and controls on recycling of older intrusive crystalline materials are unknown. This is an important problem, because this crystalline cargo carries information about the physical, chemical and thermal conditions in deeper parts of the plumbing system. For example, the preservation of Li zoning within zircons was recently interpreted to indicate that magmatic zircons spend very small amounts of their lifetime at super-solidus temperatures, indicating not only rapid remobilisation and eruption, but also rapid crystallisation following any periods of recharge, rejuvenation and melting [47].

Contrary to this, the plutonic enclaves and crystalline clots observed in Mt Lamington magmas display features of slowly-cooled magmas, including (i) the presence of melt on grain boundaries (figure 7c), (ii) rounded, poorly faceted grains, and (iii) equant grain shapes. These factors indicate slow crystal growth driven by minimisation of interfacial energies (e.g. [48,49]). Even where there is no remaining melt, the textures of interstitial plagioclase demonstrate the preservation of melt at inter-phase grain boundaries until late in crystallisation (figure 7b). From a mechanical standpoint, a crystal mush with rounded grains and melt films on grain boundaries will be readily remobilised by small degrees of re-melting and textural readjustments including mush dilation or melt infiltration (e.g. [50]; Figure 6). Conversely, faster solidification of a crystal mush will result in the formation of faceted, elongate grains that retain melt in triangular pore spaces, while interactions between neighbouring grains results in solid, interpenetrating grain boundaries (Figure 6). The higher aspect ratio of the crystals means that the rapidly solidified mush will reach its mechanical jamming threshold at higher porosity, and the solid, interpenetrating grain boundaries may require significant re-melting before adjacent grains can undergo differential movement and remobilisation. This would result in a significantly higher energy budget to enable remobilisation [51]. It is therefore possible that the volcanic record is systematically biased towards crystal cargoes that are sampled and remobilised from slowly-cooled, lower crustal intrusive materials. More rapidly cooled, smaller-volume upper crustal materials might be expected to form textures that would discourage remobilisation. Such a bias could also depend on the maturity of a given arc system; long-lived, thermally mature arcs will provide a thermally insulated environment for crustal solidification relative to young, thermally immature arcs, and this would tend to result in slower-cooled plutonic rocks showing the sorts of grain-boundary textures shown at Mt Lamington.

The persistence of any recycled components within the volcanic record also depends on crystal size, crystal composition, and dissolution mechanism and kinetics [52]. Hydrous phases (such as amphibole) are particularly susceptible to both dehydration melting and thermal decomposition so it is important to understand and predict the possible geochemical signatures of these processes [53]. A better grasp of the

kinetics of mineral dissolution may prove important for understanding how the record of crystal mush remobilisation can influence elemental and isotopic compositions of resulting magmas, as well as understanding potential biases in the crystal record. Experimental and numerical work is now needed to develop a deeper quantitative understanding of textures and kinetics associated with primary mush crystallisation and dissolution in igneous melts and appropriate analogue materials. Such approaches offer a new way to shed light on the conditions of solidification within the crust at subduction zones.

Conclusions

Amphibole trace element geochemistry can be used to interpret the origins and differentiation mechanisms of arc magma suites, taking into account the effects of changing major element crystal chemistry on partitioning to calculate amphibole equilibrium melt (AEM) compositions. At Mt Lamington, compositional variations in amphiboles from diktytaxitic mafic enclaves reflect mixing with a dacite melt of ~68 wt% SiO_2. Oscillatory zoned MgHst amphiboles from the andesite contain a record of longer-term interactions with more primitive melts back to ~55 wt% SiO_2 and variable trace element concentration, implying significant variability of small packets of primitive melt within the magmatic system over time. Plutonic-textured enclaves show variations in amphibole geochemistry consistent with simple, *in situ* fractionation of amphibole + plagioclase + biotite ± zircon ± apatite. Similar trends are observed for the andesite, but offset to different rare earth element concentrations, indicating that these are not straight-forwardly linked by fractionation, but again reflect individual small batches of magma with variable trace element composition. Differences between AEM and whole-rock compositions for the andesite indicate assimilation of solid plagioclase and zircon residue recycled from older recycled intrusive materials. Plutonic enclaves and disaggregated glomerocrysts in the andesite commonly show rounded grains and the presence of melt films along grain boundaries, which indicates slow cooling and would significantly aid mechanical remobilisation of older intrusive materials by recharging or infiltrating melts. This raises the possibility that the volcanic record of plutonic crystallisation conditions may be inherently biased towards slower-cooled mushes. More work is now needed to understand the factors controlling the primary morphology of solidifying crystal mush in arc systems.

Additional Information

Acknowledgments
We acknowledge Chris Hayward at the University of Edinburgh for assistance with the acquisition of electron microprobe data that support this manuscript. We also thank Richard Arculus for his generous loan of sample materials for this project. We gratefully acknowledge the comments of an anonymous reviewer, and a particularly thorough and helpful review from Szabolcs Harangi.

Funding Statement
MCSH acknowledges support from a Royal Society University Research Fellowship. This work originated as part of the PhD thesis of Jing Zhang, which was supported by the China Scholarship Council and a Durham Doctoral Scholarship from Durham University. George Cooper acknowledges NERC grant NE/K010824/1.

Data Accessibility
The datasets supporting this article have been uploaded as part of the Supplementary Material.

Competing Interests
We have no competing interests.

Authors' Contributions
Data acquisition and processing was conducted by JZ with the assistance of GFC and CJO. MCSH, JZ and GFC analysed the data and interpreted the results, and MCSH and GFC drafted the manuscript. All authors were involved in discussion, critical revision and final approval of the manuscript. We remember our friend and colleague Jon Davidson in the publication of this work.

References

1. Davidson, J.P., Hora, J.M., Garrison, J.M. & Dungan, M.A. (2005) Crustal forensics in arc magmas. Journal of Volcanology and Geothermal Research 140, 157-170

2. Hildreth, W. & Moorbath, S. (1988) Crustal contributions to arc magmatism in the Andes of Central Chile. Contributions to Mineralogy and Petrology 98, 455-489
3. Annen, C., Blundy, J.D. & Sparks, R.S.J. (2006) The genesis of intermediate and silicic magmas in deep crustal hot zones. Journal of Petrology 47 (3), 505-539
4. Humphreys, M.C.S., Blundy, J.D. & Sparks, R.S.J. (2006) Magma evolution and open-system processes at Shiveluch Volcano: Insights from phenocryst zoning. Journal of Petrology 47 (12), 2303-2334
5. Eichelberger, J.C., Izbekov, P.E. & Browne, B.L. (2006) Bulk chemical trends at arc volcanoes are not liquid lines of descent. Lithos 87, 135-154
6. Straub, S.M., Gomez-Tuena, A., Stuart, F.M., Zellmer, G.F., Espinasa-Perena, R., Cai, Y. & Iizuka, Y. (2011) Formation of hybrid arc andesites beneath thick continental crust. Earth and Planetary Science Letters 303, 337-347
7. Jerram, D.A. & Martin, V.M. (2008) Understanding crystal populations and their significance through the magma plumbing system. *In: Annen, C. & Zellmer, G.F. (eds)* Dynamics of Crustal Magma Transfer, Storage and Differentiation. Geological Society, London, Special Publications, 304, 133–148.
8. Hildreth, W. & Wilson, C.J.N. (2007) Compositional zoning of the Bishop Tuff. Journal of Petrology 48 (5) 951-999
9. Pichavant, M., Costa, F., Burgisser, A., Scaillet, B., Martel, C. & Poussineau, S. (2007) Equilibration scales in silicic to intermediate magmas – implications for experimental studies. Journal of Petrology 48 (10), 1955-1972
10. Bachmann, O. & Bergantz, G.W. (2006) Gas percolation in upper-crustal silicic crystal mushes as a mechanism for upward heat advection and rejuvenation of near-solidus magma bodies. Journal of Volcanology and Geothermal Research 149, 85-102
11. Cashman, K. & Sparks, R.S.J. (2013) How volcanoes work: A 25 year perspective. Geological Society of America Bulletin doi: 10.1130/B30720.1
12. Burgisser, A. & Bergantz, G.W. (2011) A rapid mechanism to remobilize and homogenize highly crystalline magma bodies. Nature 471, 212-215
13. Barboni, M., Boehnke, P., Schmitt, A.K., Harrison, T.M., Shane, P., Bouvier, A.-S. & Baumgartner, L. (2016) Warm storage for arc magmas. PNAS 113 (49), 13959-13964
14. Miller, J.S., Matzel, J.E.P., Miller, C.F., Burgess, S.D. & Miller, R.B. (2007) Zircon growth and recycling during the assembly of large, composite arc plutons. Journal of Volcanology and Geothermal Research 167 (1-4), 282-299. doi: 10.1016/j.jvolgeores.2007.04.019
15. Bégué, F., Deering, C.D., Gravley, D.M., Kennedy, B.M., Chambefort, I., Gualda, G.A.R. & Bachmann, O. (2014) Extraction, storage and eruption of multiple isolated magma batches in the paired Mamaku and Ohakuri eruption, Taupo Volcanic Zone, New Zealand. Journal of Petrology 55 (8), 1653-1684
16. Kent, A.J.R. (2014) Preferential eruption of andesitic magmas: Implications for volcanic magma fluxes at convergent margins. Geological Society, London, Special Publications 385, 257-280
17. Christopher, T.E., Blundy, J., Cashman, K., Cole, P., Edmonds, M., Smith, P.J., Sparks, R.S.J. & Stinton, A. (2015) Crustal-scale degassing due to magma system destabilization and magma-gas decoupling at Soufriere Hills Volcano, Montserrat. Geochemistry, Geophysics, Geosystems 16, doi: 10,1002/2015GC005791
18. Cooper, K.M. (2015) Timescales of crustal magma reservoir processes: insights from U-series crystal ages. *In:* Caricchi, L. & Blundy, J.D. (eds) *Chemical, Physical and temporal evolution of magmatic systems*. Geological Society, London, Special Publications 422, 141-174
19. Cashman, K. & Blundy, J. (2013) Petrological cannibalism: the chemical and textural consequences of incremental magma body growth. Contributions to Mineralogy and Petrology 166 (3), 703-729
20. Johnson, R.W., Mackenzie, D.E. & Smith, I.E.M. (1978) Volcanic rock associations at convergent plate boundaries: Reappraisal of the concept using case histories from Papua New Guinea. Geological Society of America Bulletin 89, 96-106
21. Zhang, J, Davidson, J.P., Humphreys, M.C.S., Macpherson, C.G. & Neill, I. (2015) Magmatic Enclaves and Andesitic Lavas from Mt. Lamington, Papua New Guinea: Implications for Recycling of Earlier-fractionated Minerals through Magma Recharge. Journal of Petrology 56 (11), 2223-2256
22. Taylor, G.A. (1958) The 1951 eruption of Mount Lamington, Papua. Bureau of Mineral Resources, Geology and Geophysics Bulletin 38
23. Arculus, R.J., Johnson, R.W., Chappell, B.W., McKee, C.O. & Sakai, H. (1983) Ophiolite-contaminated andesite, trachybasalts and cognate inclusions of Mount Lamington, Papua New Guinea: anhydrite-amphibole-bearing lavas and the 1951 cumulodome. Journal of Volcanology and Geothermal Research 18, 215-247
24. Hall, R. & Spakman, W. (2002) Subducted slabs beneath the eastern Indonesia-Tonga region: insights from tomography. Earth and Planetary Science Letters 201 (2), 321-336
25. Johnson, R.W., Mackenze, D.E. & Smith, I.E.M. (1978) Delayed partial melting of subduction-modified mantle in Papua New Guinea. Tectonophysics 46 (1-2), 197-216
26. England, R.N. & Davies, H.L. (1973) Mineralogy of ultramafic cumulates and tectonics from eastern Papua. Earth and Planetary Science Letters 17 (2), 416-425

27. Jacques, A.L. & Chappell, B.W. (1980) Petrology and trace element geochemistry of the Papuan ultramafic belt. Contributions to Mineralogy and Petrology 75 (1), 55-70
England, R.N. & Davies, H.L. (1973) Mineralogy of ultramafic cumulates and tectonites from eastern Papua. Earth and Planetary Science Letters 17 (2), 416-425
28. Paton, C., Hellstrom, J., Paul, B., Woodhead, J. & Hergt, J. (2011) Iolite: Freeware for the visualization and processing of mass spectrometric data. Journal of Analytical Atomic Spectrometry, 26 (12), 2508. doi:10.1039/c1ja10172b
29. Hellstrom, J., Paton, C., Woodhead, J.D. & Hergt, H.M. (2008) Iolite software for spatially resolved LA-(quad and MC) IPCMS analysis. In Laser Ablation ICP-MS in the Earth Sciences: Current Pratices and Outstanding Issues (P. Sylvester, ed). Mineralogical Association of Canada Short Course series 40, p343.
30. Humphreys, M.C.S., Cooper, G.F., Zhang, J., Loewen, M., Kent, A.J.R., Macpherson, C.G. & Davidson, J.P. (in review). Amphibole reveals the hidden complexity of lower crustal magma plumbing systems as arcs. Contributions to Mineralogy and Petrology (in review)
31. Leake, B.E., Woolley, A.R., Arps, C.E.S., Birch, W.D., Gilbert, M.C., Grice, J.D., Hawthorne, F.C., Kato, A. Kisch, H.J., Krivovichev, V.G., Linthout, K., Laird, J., Mandarino, J.A., Maresch, W.V., Nickel, E.H., Rock, N.M.S., Schumacher, J.C., Smith, D.C., Stephenson, N.C.N., Ungaretti, L., Whittaker, E.J.W. & Youzhi, G. (1997) Nomenclature of amphiboles: report of the subcommittee on amphiboles of the international mineralogical Association, Commission on New Minerals and Mineral Names. Canadian Mineralogist 35, 219-246
32. Zhang, J., Humphreys, M.C.S., Cooper, C.F., Davidson, J.P. & Macpherson, C.G. (2017) Magma mush chemistry at subduction zones, revealed by new melt major element inversion from calcic amphiboles. American Mineralogist 102 (6), 1353-1367
33. Blundy, J.D. & Wood, B.J. (1991) Crystal-chemical controls on the partitioning of Sr and Ba between plagioclase feldspar, silicate melts, and hydrothermal solutions. Geochimica et Cosmochimica Acta 55, 193-209
34. Kiss, B., Harangi, S., Ntaflos, T., Mason, P.R.D., Pál-Molnár, E. (2014) Amphibole perspective to unravel pre-eruptive processes and conditions in volcanic plumbing systems beneath intermediate arc volcanoes: a case study from Ciomadul volcano (SE Carpathians). Contributions to Mineralogy and Petrology 167, 986
35. Watson, E.B. & Harrison, T.M. (1983) Zircon saturation revisited: temperature and composition effects in a variety of crustal magma types. Earth and Planetary Science Letters 64, 295-304
36. Maclennan, J. (2008) Concurrent mixing and cooling of melts under Iceland. Journal of Petrology 49 (11) 1931-1953
37. Cooper, G.F. & Wilson, C.J.N. (2014) Development, mobilization and eruption of a large crystal-rich rhyolite: the Ongatiti ignimbrite, New Zealand. Lithos 198-199, 38-57
38. Blatter, D.L., Sisson, T.W. & Hankins, W.B. (2017) Voluminous arc dacites as amphibole reaction-boundary liquids. Contributions to Mineralogy and Petrology 172, 27
39. Davidson, J., Turner, S., Handley, H. Macpherson, C. & Dosseto, A. (2007) Amphibole “sponge” in arc crust? Geology 35 (9) 787-790
40. Li, L., Xiong, X.L. & Liu, X.C. (2017) Nb/Ta Fractionation by Amphibole in Hydrous Basaltic Systems: Implications for Arc Magma Evolution and Continental Crust Formation. Journal of Petrology 1-26, doi: 10.1093/petrology/egw070
41. Arculus, R.J. & Wills, K.J.A. (1980) The petrology of plutonic blocks and inclusions from the Lesser Antilles island arc. Journal of Petrology 21 (4) 743-799
42. Smith, D.J. (2014) Clinopyroxene precursors to amphibole sponge in arc crust. Nature Communications 5: 4329
43. Cooper, G.F., Davidson, J.P. & Blundy, J.D. (2016) Plutonic xenoliths from Martinique, Lesser Antilles: evidence for open system processes and reactive melt flow in island arc crust. Contributions to Mineralogy and Petrology 171: 87
44. Klaver, M., Matveev, S., Berndt, J., Lissenberg, C.J. & Vroon, P.Z. (2017) A mineral and cumulate perspective to magma differentiation at Nisyros volcano, Aegean arc. Contributions to Mineralogy and Petrology 172: 95
45. Kay, R.W. (1978) Aleutian magnesian andesites: melts from subducted Pacific ocean crust. Journal of Volcanology and Geothermal Research 4, 117-132
46. Arth, J.G. & Barker, F. (1976). Rare-earth partitioning between hornblende and dacitic liquid and implications for the genesis of trondhjemitic-tonalitic magmas. Geology 4, 534-536
47. Rubin, A.E., Cooper, K.M., Till, C.B., Kent, A.J.R., Costa, F., Bose, M., Gravley, D., Deering, C. & Cole, J. (2017) Rapid cooling and cold storage in a silicic magma reservoir recorded in individual crystals. Science 356 (6343) 1154-1156
48. Bulau, J.R., Waff, H.S. & Tyburczy, J.A. (1979) Mechanical and thermodynamic constraints on fluid distribution in partial melts. Journal of Geophysical Research 84 (B11) 6102-6108
49. Holness, M.B., Humphreys, M.C.S, Sides, R., Helz, R.T. & Tegner, C. (2012) Toward an understanding of disequilibrium dihedral angles in mafic rocks. Journal of Geophysical Research 117, B06207

50. Shibano, Y., Namiki, A. & Sumita, I. (2012) Experiments on upward migration of a liquid-rich layer in a granular medium: Implications for a crystalline magma chamber. Geochemistry, Geophysics, Geosystems 13 (3), Q03007
51. Spera, F.J. & Bohrson, W.A. (2018) Rejuvenation of crustal magma mush: a tale of multiply nested processes and timescales. American Journal of Science 318, 90-140
52. Bindeman, I.N. & Melnik, O.E. (2016) Zircon survival, rebirth and recycling during crustal melting, magma crystallization, and mixing based on numerical modelling. Journal of Petrology 57 (3), 437-460
53. Brophy, J.G. (2008) A study of rare earth element (REE)–SiO_2 variations in felsic liquids generated by basalt fractionation and amphibolite melting: a potential test for discriminating between the two different processes. Contributions to Mineralogy and Petrology 156, 337-357

Figure and table captions

Figure 1
Amphibole major element compositions from the andesite (including MgHbl-Tsch and MgHst), diktytaxitic enclaves and plutonic enclave. Trachybasalt amphibole compsitions are shown for comparison (data from [21, 23]). (a) Mg# = Mg/(Mg+Fe^{tot}) vs Al_{tot} (following [34]). Arrows and outline fields show effect of varying temperature, pressure and melt composition in experimental results as summarised by [34]. (b) K_2O vs TiO_2 concentrations.

Figure 2
Trace element compositions of amphibole equilibrium melts (AEM), calculated following Humphreys et al. (in review; see also supplementary information). SiO_2 of AEM are calculated using Zhang et al. (2017). Whole-rock compositions are shown for comparison. Grey bars in (c) indicate Sr concentrations of plagioclase equilibrium melts from cores and rims of microphenocrysts from the diktytaxitic enclaves. Error bars show representative 2σ regression uncertainties for the MgHbl. The dotted outline marks the diktytaxitic enclaves whole rocks.

Figure 3
Trace element ratios of amphibole equilibrium melts (AEM, calculated following [30]) plotted against SiO_2 of AEM, calculated following [32]. Europium anomaly in (b) is calculated from $EuN/\sqrt{(Sm_N*Gd_N)}$ where N denotes chondrite-normalised compositions. In (c) and (d) the dashed line marks the approximate composition of the putative dacite melt. The diktytaxitic enclave AEM form by mixing with dacitic melt, while the plutonic and andesite AEM trends are dominated by fractionation. The dotted outline marks the diktytaxitic enclaves.

Figure 4
Chondrite-normalised rare earth element profiles for amphibole equilibrium melts (AEM) from the diktytaxitic mafic enclaves plutonic-textured enclave, and andesite. Whole rock compositions are shown in the light grey bar (andesite) and dark grey region (diktytaxitic mafic enclaves). In (d), spiky MgHst are shown with long-dashed orange lines; diffuse-textured MgHst with purple dotted lines.

Figure 5
Trace element contents of plagioclase from the andesite, microphenocrysts from the diktytaxitic mafic enclaves, and plutonic-textured enclave, together with the compositions of sieve-textured crystal rims. Data from [21].

FIgure 6
Sketch of primary mush textures during slow cooling (a) and faster cooling (c). Slow cooling results in rounded, equant grains and retention of melt on grain boundaries. Faster cooling results in higher aspect ratio grains and solid, knitted grain boundaries. Mechanical remobilisation and recycling of the slower-cooled mush (b) requires only dilation and/or grain rotation and little re-melting. In contrast, mechanical remobilisation or recycling of the faster cooled mush (d) requires significant extents of remelting. See text for details.

Figure 7
Textural features of magmatic products from Mt Lamington. (a) Clusters of amphibole ± biotite ± Cr-rich oxide inclusions, representing fully reacted olivine antecrysts, plane polarised light. (b) Small-scale changes in extinction angle of plagioclase at the margins of interstitial grains where they border amphibole (arrows), indicating late-stage retention of melt along these boundaries; cross-polarised light. (c) BSE image showing interstitial growth of biotite at low undercooling, resulting in rounded interfaces and retention of melt on the

grain boundaries (bi = biotite, hbl = hornblende, gl = glass, v = vesicle). (d) BSE image of amphibole glomerocryst, interpreted to have been disaggregated from plutonic enclave material prior to eruption. The glomerocryst has a late-stage overgrowth rim of darker amphibole.

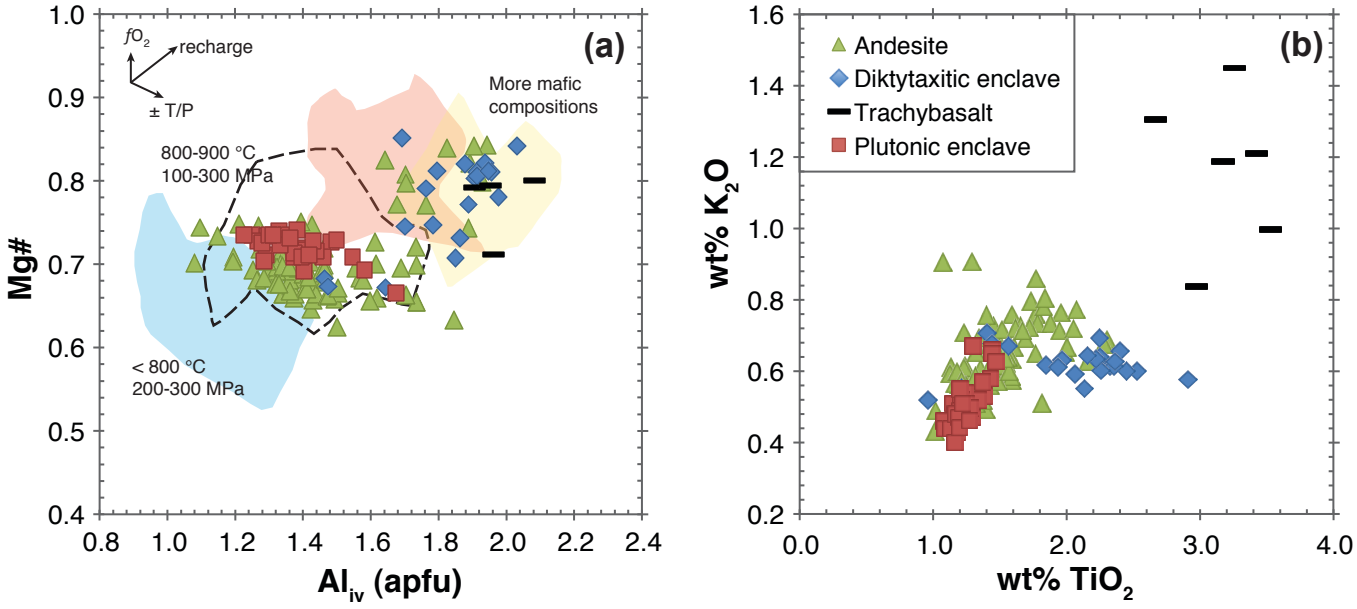

Figure 1
Amphibole major element compositions from the andesite (including MgHbl-Tsch and MgHst), diktytaxitic enclaves and plutonic enclave. Trachybasalt amphibole compsitions are shown for comparison (data from Zhang et al. 2015; Arculus et al. 1983). (a) Mg# = Mg/(Mg+Fe^{2+}) vs Al^{iv} (following Kiss et al. 2014). Arrows and outline fields show effect of varying temperature, pressure and melt composition in experimental results as summarised by Kiss et al. (2014). (b) K_2O vs TiO_2 concentrations.

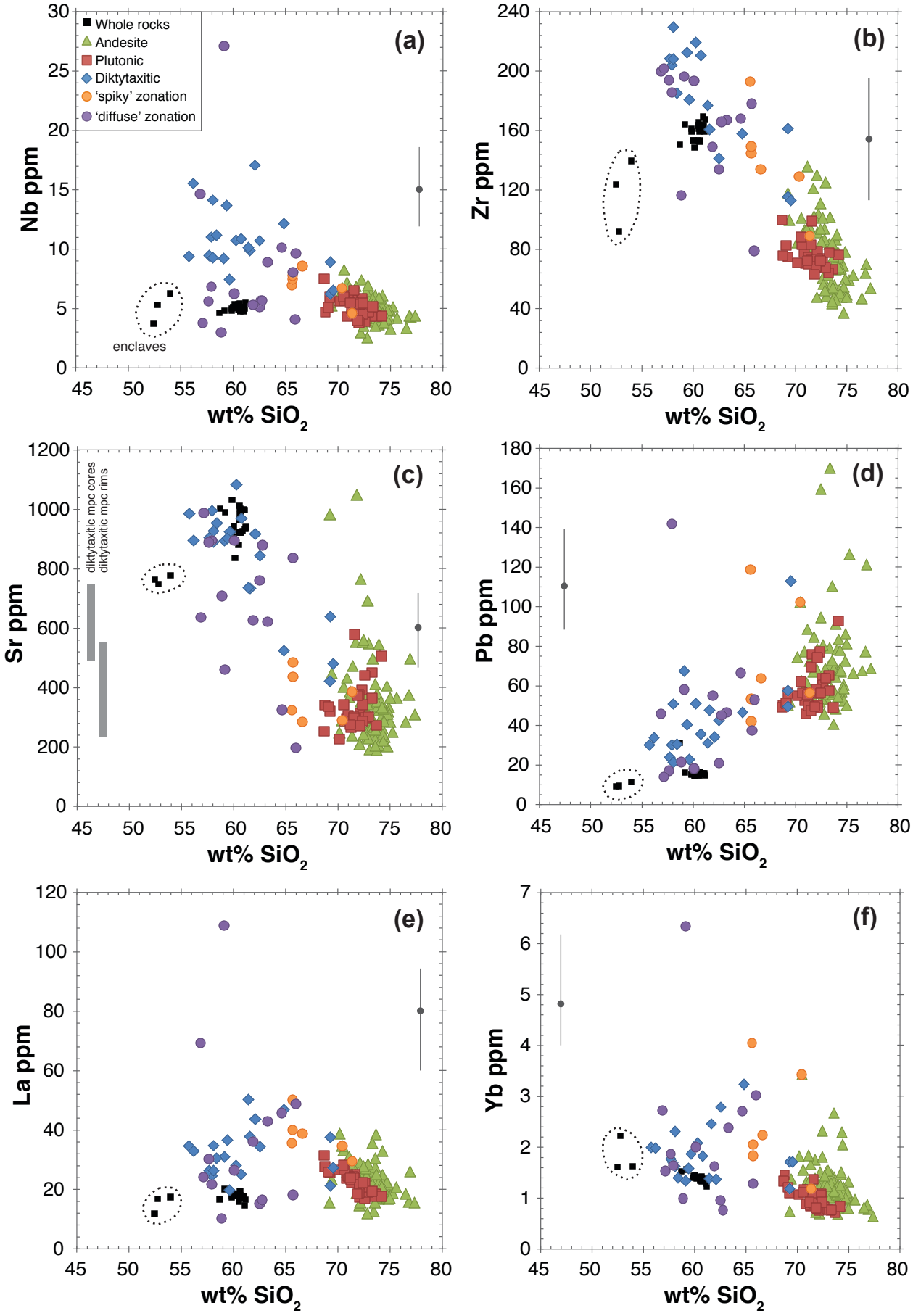

Figure 2

Trace element compositions of amphibole equilibrium melts (AEM), calculated following Humphreys et al. (in review; see also supplementary information). SiO_2 of AEM are calculated using Zhang et al. (2017). Whole-rock compositions are shown for comparison. Grey bars in (c) indicate Sr concentrations of plagioclase equilibrium melts from cores and rims of microphenocrysts from the diktytaxitic enclaves. Error bars show representative 2σ regression uncertainties for the MgHbl. The dotted outline marks the diktytaxitic enclaves whole rocks.

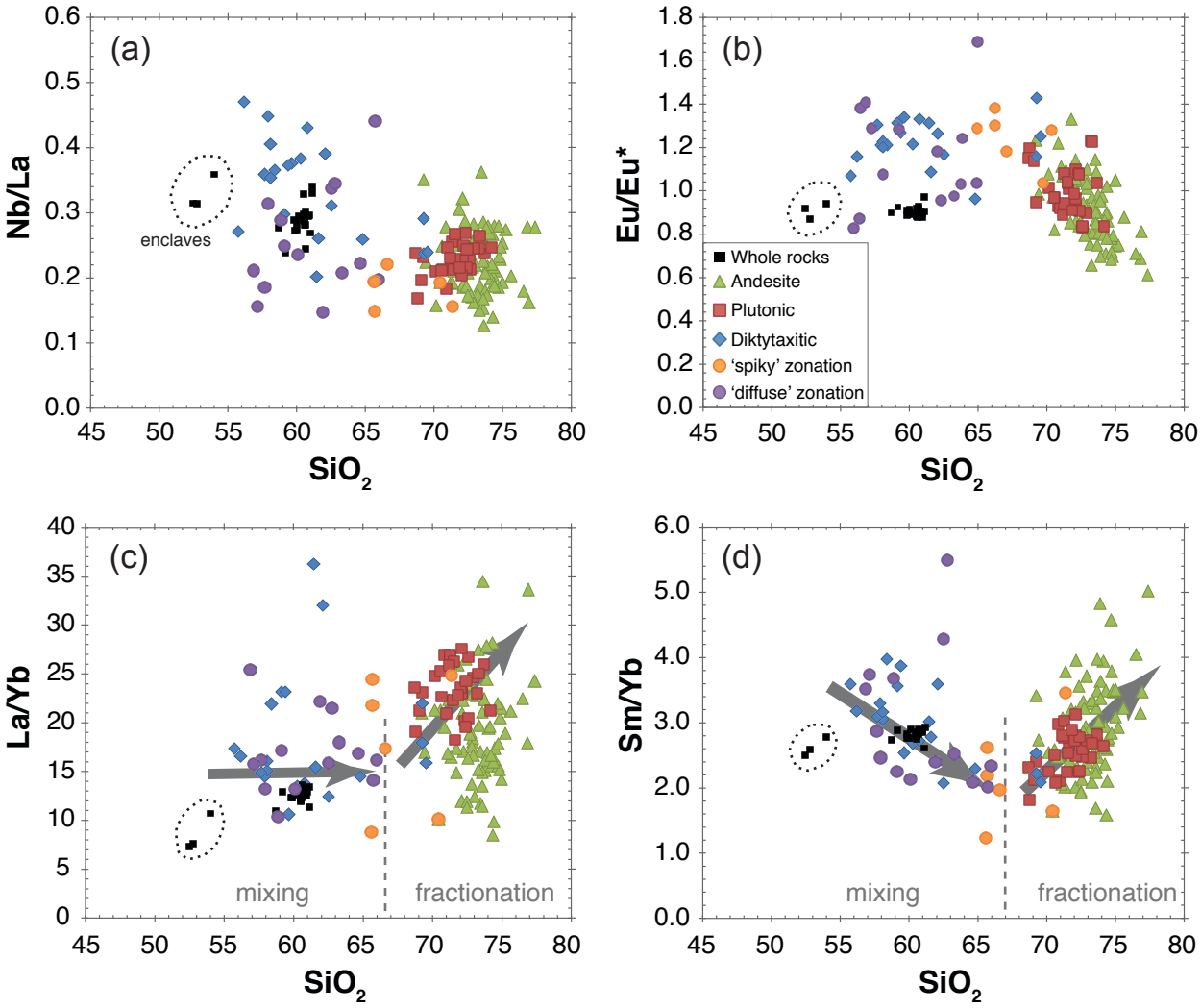

Figure 3
Trace element ratios of amphibole equilibrium melts (AEM, calculated following Humphreys et al. in review) plotted against SiO_2 of AEM, calculated following Zhang et al. (2017). Europium anomaly in (b) is calculated from $Eu_N/\sqrt{(Sm_N*Gd_N)}$ where N denotes chondrite-normalised compositions. In (c) and (d) the dashed line marks the approximate composition of the putative dacite melt. The diktytaxitic enclave AEM form by mixing with dacitic melt, while the plutonic and andesite AEM trends are dominated by fractionation. The dotted outline marks the diktytaxitic enclaves.

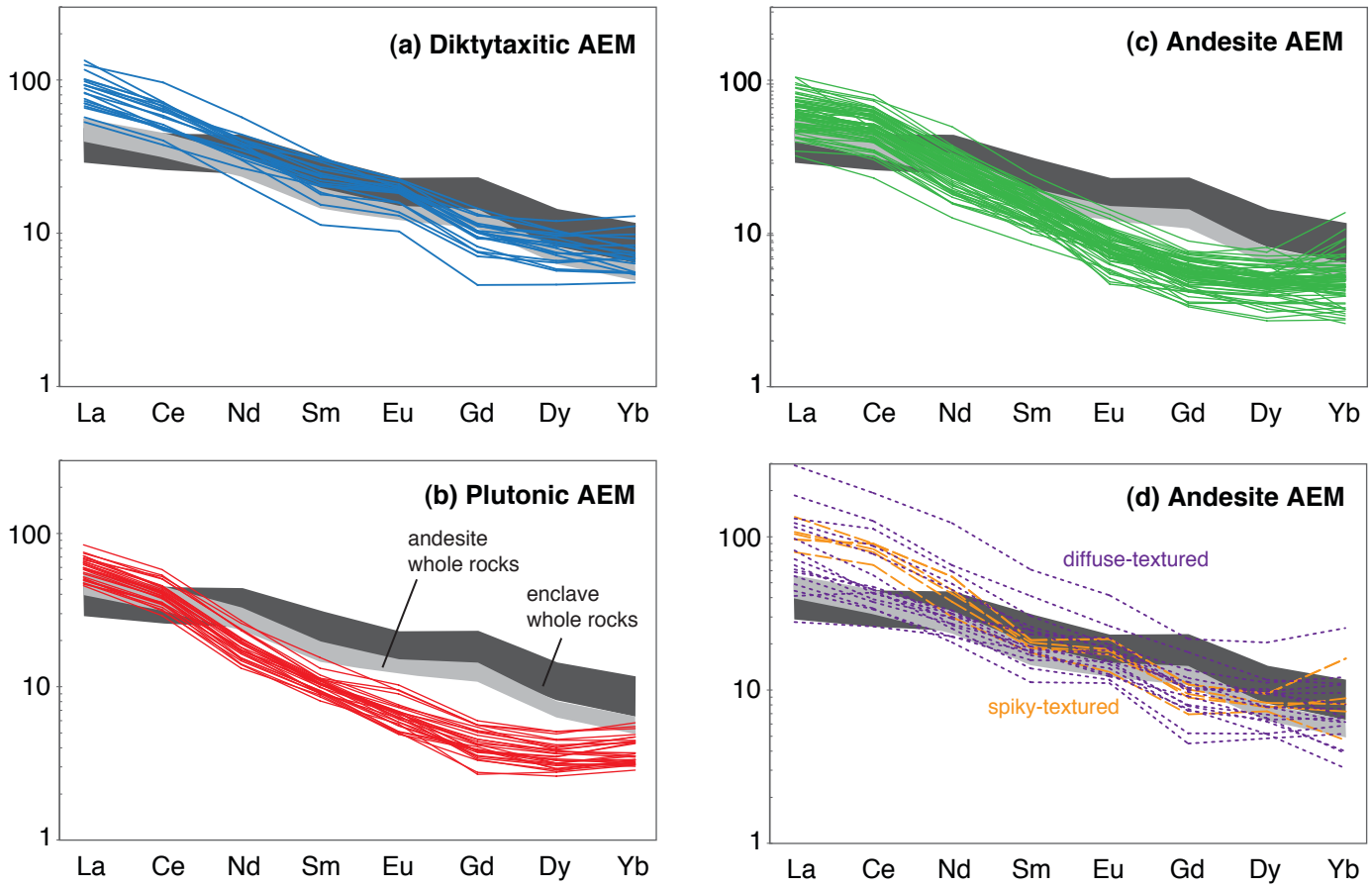

Figure 4
Chondrite-normalised rare earth element profiles for amphibole equilibrium melts (AEM) from the diktytaxitic mafic enclaves plutonic-textured enclave, and andesite. Whole rock compositions are shown in the light grey bar (andesite) and dark grey region (diktytaxitic mafic enclaves). In (d), spiky MgHst are shown with long-dashed orange lines; diffuse-textured MgHst with purple dotted lines.

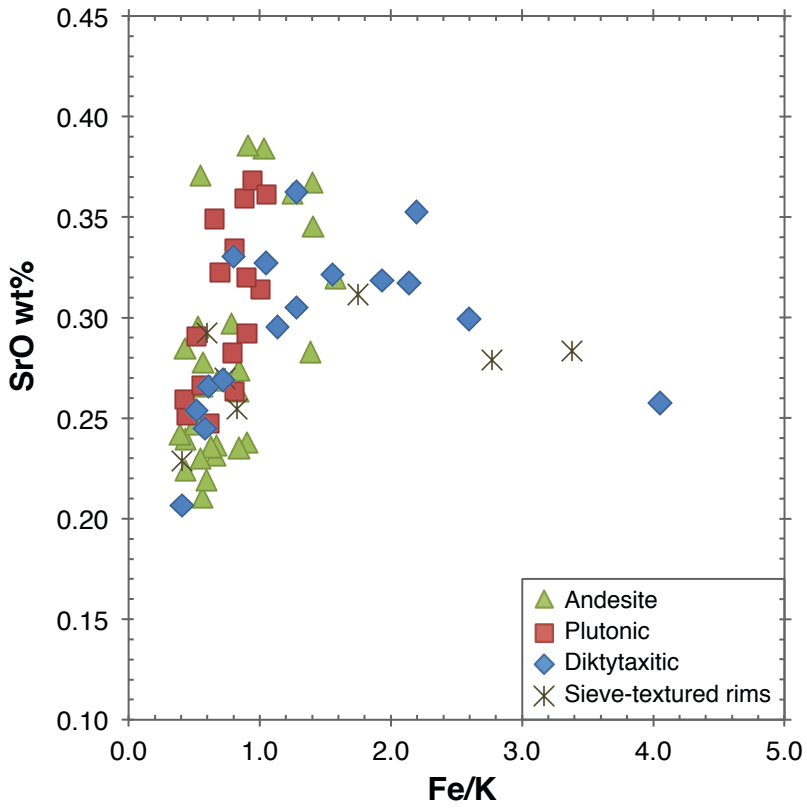

Figure 5
Trace element contents of plagioclase from the andesite, microphenocrysts from the diktytaxitic mafic enclaves, and plutonic-textured enclave, together with the compositions of sieve-textured crystal rims. Data from Zhang et al (2015).

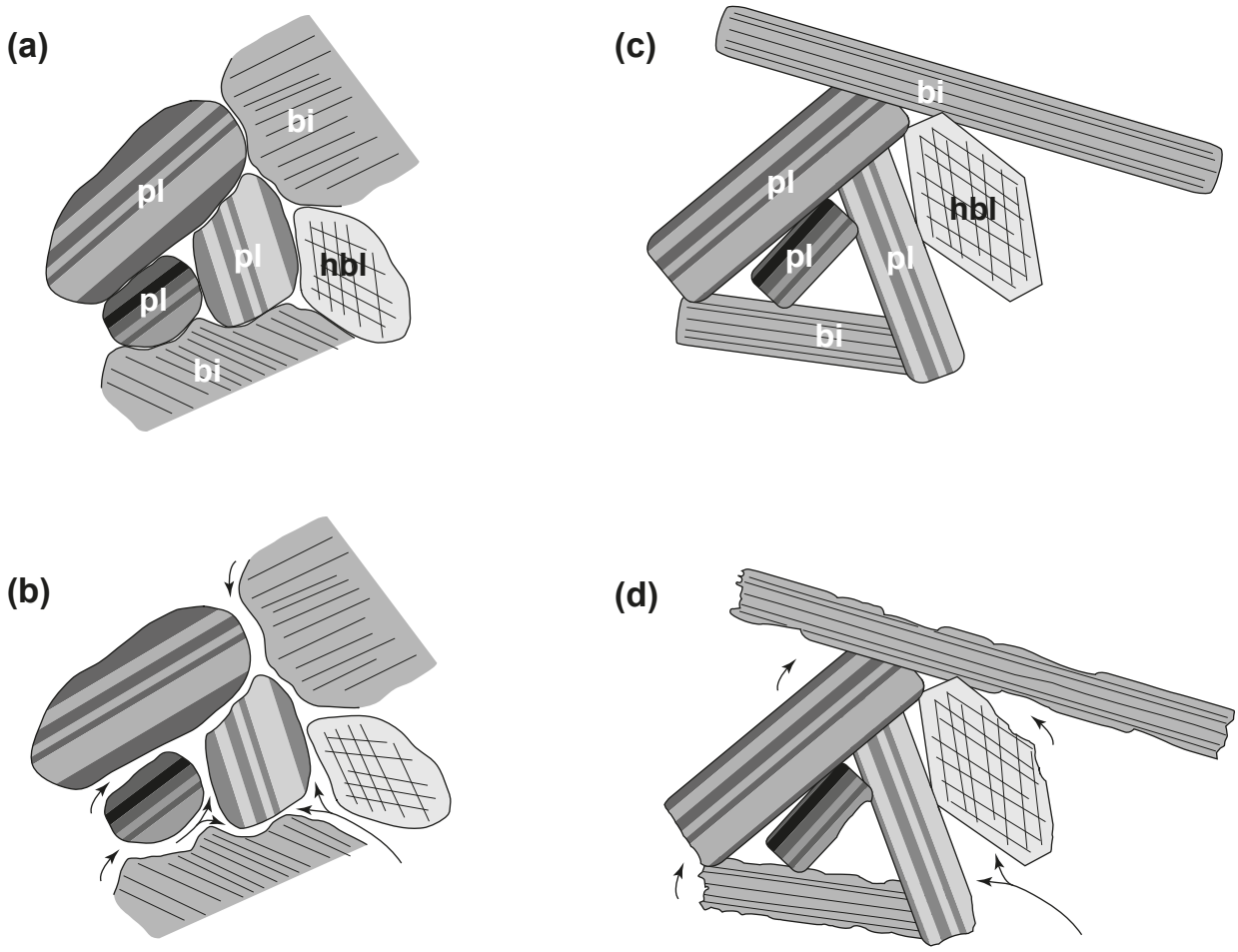

FIgure 6
Sketch of primary mush textures during slow cooling (a) and faster cooling (c). Slow cooling results in rounded, equant grains and retention of melt on grain boundaries. Faster cooling results in higher aspect ratio grains and solid, knitted grain boundaries. Mechanical remobilisation and recycling of the slower-cooled mush (b) requires only dilation and/or grain rotation and little re-melting. In contrast, mechanical remobilisation or recycling of the faster cooled mush (d) requires significant extents of remelting. See text for details.

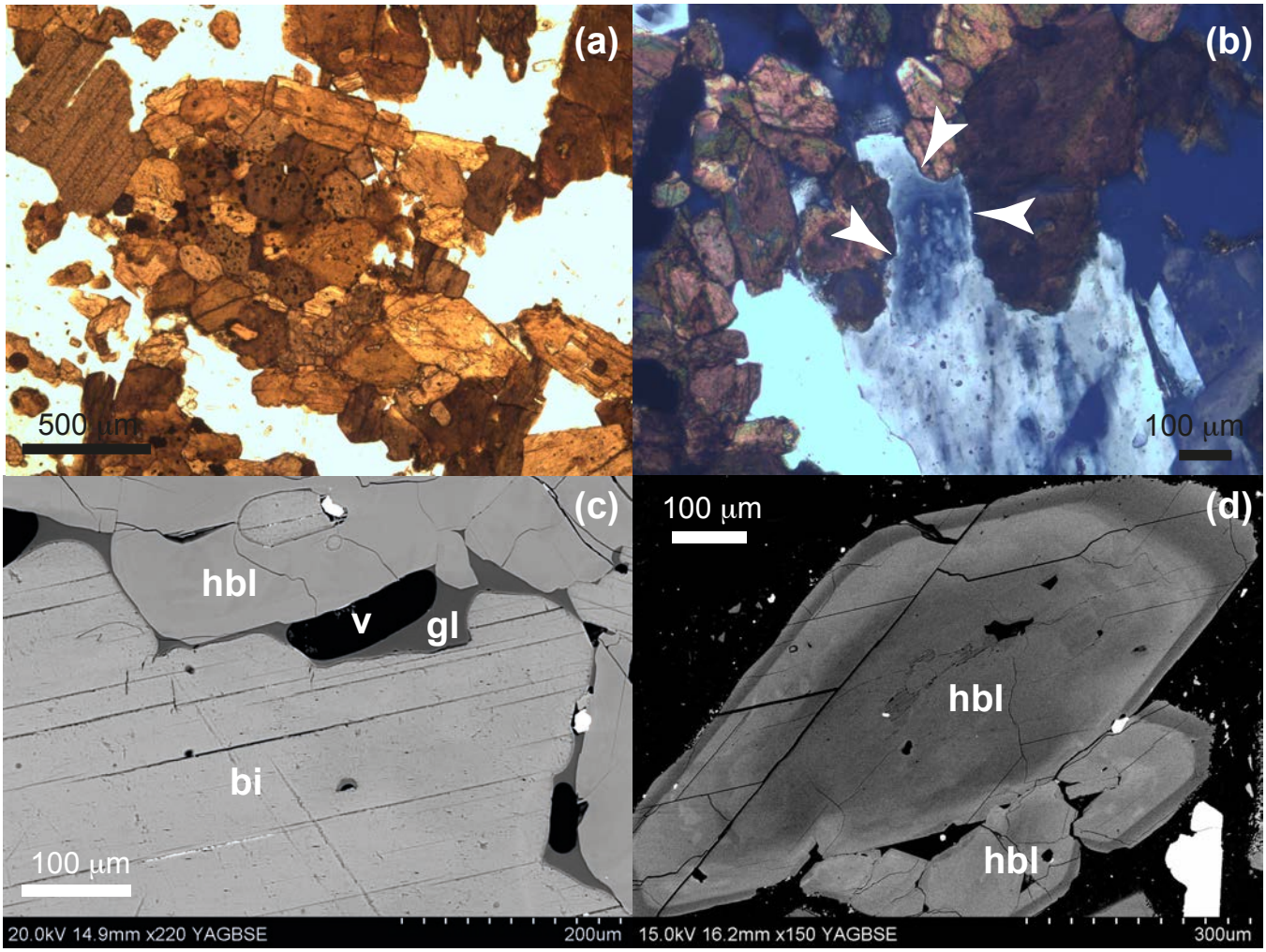

Figure 7
Textural features of magmatic products from Mt Lamington. (a) Clusters of amphibole ± biotite ± Cr-rich oxide inclusions, representing fully reacted olivine antecrysts, plane polarised light. (b) Small-scale changes in extinction angle of plagioclase at the margins of interstitial grains where they border amphibole (arrows), indicating late-stage retention of melt along these boundaries; cross-polarised light. (c) BSE image showing interstitial growth of biotite at low undercooling, resulting in rounded interfaces and retention of melt on the grain boundaries (bi = biotite, hbl = hornblende, gl = glass, v = vesicle). (d) BSE image of amphibole glomerocryst, interpreted to have been disaggregated from plutonic enclave material prior to eruption. The glomerocryst has a late-stage overgrowth rim of darker amphibole.

Supplementary information

Summary of trace element partitioning regression procedure

The crystal structure of amphibole includes several crystallographic sites with different coordination and size that can accommodate a range of trace elements, including large ion lithophile elements (Rb, Sr, Ba), Pb, U, Th, high field strength elements (Ti, Zr, Hf, Nb and Ta), rare earth elements (REE) and Y, and transitional metals (e.g. Tiepolo et al. 2007). Elements with large ionic radius (e.g. Rb, Pb) are accommodated in the A site, while highly charged high-field strength elements (e.g. Zr^{4+}) substitute for Ti on the M2 site (Oberti *et al.*, 2000), and REE and Y partition onto the M4 site (Brenan et al. 1995; Klein et al. 1997; Hilyard et al. 2000; Shimizu et al. 2017). To account for the strong crystal-chemical control on partitioning, we used multiple regression (MR) methods to predict amphibole-melt trace element partition coefficients from the major element composition of the crystal, using a compilation of 13 published high-temperature experimental studies. These studies covered a wide range of conditions (200-2,500 MPa, 780-1,100 °C) and melt compositions (basanite to rhyolite) and crystallised calcic amphiboles (pargasite – edenite – hastingsite – magnesiohastingsite – kaersutite – tschermakite – magnesiohornblende). Temperature was not included as an independent variable. Amphibole formula components were used as independent variables, including Si_T; Al_{VI}; M1-3 site Ti, Fe^{3+}, and Fe^{2+}; Ca_{M4}; and Na_A. We calculated the 'average Fe^{3+}' stoichiometry following Leake et al. (1997). See Humphreys et al. (in review) for further details. For major elements, we used a revised form of the major element regression scheme of Zhang et al. (2017).

References

Tiepolo, M., Oberti, R. & Zanetti, A. (2007) Trace-element partitioning between amphibole and silicate melt. Reviews in Mineralogy and Geochemistry 67, 417–452

Oberti, R., Vannucci, R., Zanetti, A., Tiepolo, M. & Brumm, R.C. (2000) A crystal chemical re-evaluation of amphibole/melt and amphibole/clinopyroxene D_{Ti} values in petrogenetic studies. American Mineralogist, 85, 407-419

Brenan J.M., Shaw H.F., Ryerson F.J. & Phinney D.L. (1995) Experimental determination of trace-element partitioning between pargasite and a synthetic hydrous andesitic melt. Earth and Planetary Science Letters 135, 1–11

Klein, M., Stosch, H.-G., Seck, H.A. (1997) Partitioning of high field-strength and rare-earth elements between amphibole and quartz-dioritic to tonalitic melts: an experimental study. Chemical Geology 138, 257–271

Hilyard, M., Nielsen, R.L., Beard, J.S. et al (2000) Experimental determination of the partitioning behaviour of rare earth and high field strength elements between pargasitic amphibole and natural silicate melts. Geochimica et Cosmochimica Acta 64, 1103–1120

Shimizu, K., Liang, Y., Sun, C., Jackson, C.R.M. & Saal, A.E. (2017) Parameterized lattice strain models for REE partitioning between amphibole and silicate melt. American Mineralogist 102, 2254–2267

Leake, B.E., Woolley, A.R., Arps, C.E.S., et al (1997) Nomenclature of amphiboles: report of the subcommittee on amphiboles of the International Mineralogical Association, Commission on New Minerals and Mineral Names. Canadian Mineralogist 35, 219–246

Humphreys, M.C.S., Cooper, G.F., Zhang, J., Loewen, M., Kent, A.J.R., Macpherson, C.G. & Davidson, J.P. (in review) Amphibole reveals the hidden complexity of lower crustal magma plumbing systems at arcs. Contributions to Mineralogy and Petrology (in review)

Regression equations used to calculate major element amphibole equilibrium melts (AEM), after Zhang et al. (2017); Zhang et al. (erratum). An example is given below the table. The parameter "lnSiPoly" is equivalent to a polynomial of the tetrahedral Si content:

$\ln SiPoly = -164.73*\ln Si_T^2 + 757.99*\ln Si_T - 772.44$

Results of multiple linear regressions used for estimating melt major element compositions on the basis of temperature and calcic-amphibole component. N = 130

Eq.	Dependent variable	Parameters used	Range of variation	Constant	Si	lnSiPoly	Al (vi)	Mg	Fe3+	Fe2+	Ti	Ca	Na (A)	*Multiple R^2*	*SE (wt %)*	*se (wt%)*
1	SiO_2 (wt %)	lnSiPoly	39.6 - 79.2	-138.2109		1.5533	19.9584		30.2722	7.3331	44.9836	36.5966		0.839	3.73	5.31
				± 25.3058		*± 0.1298*	*± 4.4996*		*± 4.4616*	*± 0.8076*	*± 9.1473*	*± 7.4745*				
4	$lnTiO_2$	Si_T	-2.8 - 1.8	19.1540	-2.7852			1.0678	-1.6996			-2.2233	-1.6150	0.825	0.64	0.39
				± 1.16484	*± 0.16672*			*± 0.07654*	*±0.19083*			*± 0.49808*	*± 0.41673*			
7	lnFeO	Si_T, Fe_T	-0.34 - 2.75	16.5023	-2.1604			0.2928				-1.4158		0.705	2.18	2.71
				± 1.1184	*± 0.1261*			*± 0.0734*				*± 0.4284*				
8	lnMgO	Si_T	-2.19 - 2.47	12.9140	-2.6555		1.0045	1.2374						0.800	1.12	1.28
				± 0.93019	*± 0.14592*		*± 0.27452*	*±0.07951*								
9	lnCaO	Si_T, Fe_T	-2.19 - 2.47	6.2200	-1.1514		1.2727	0.6931						0.708	1.45	1.94
				± 0.61322	*± 0.09619*		*± 0.18097*	*± 0.05241*								
10	K_2O (wt %)	Si_T	<6.0	31.6434	-2.6611		-6.4625	-1.3486	-5.0597		-6.1714		-5.7344	0.586	0.76	0.91
				± 5.4085	*± 0.6548*		*± 0.8317*	*± 0.1607*	*± 0.7102*		*± 1.3617*		*± 0.9997*			
11	Al2O3	Si_T	11.4 - 21.5	29.8766	-2.5551		2.9594						4.8840	0.530	1.31	1.45
				± 4.1070	*± 0.5681*		*± 0.8313*						*± 1.2277*			

Normal font indicates p-value < 0.01; bold font indicates the *p-value* of the parameter or the constant is 0.01 ≤ *p-value* < 0.05

e.g. $lnTiO_2$ (wt%) = 19.1540 - 2.7852*Si + 1.0678*Mg - 1.6996*Fe^{3+} - 2.2233*Ca - 1.6150*Na_A

Regression equations used to calculate trace element amphibole equilibrium melts (AEM), after Humphreys et al. (in review). An example is given below the table.

	Intercept	Si	Al_{IV}	Ti	Fe^{3+}	Fe^{2+}	Ca	NaA	SE	R^2
lnDRb	9.1868	-1.3898		-3.6797	-1.5769	-0.6938			0.286	0.85
±	2.4481	0.3989		0.629	0.4764	0.16				
lnDSr	3.41585	-0.75281				0.36529			0.191	0.64
±	0.84461	0.13988				0.05751				
lnDPb	-4.2533		2.7155	1.69	0.7065			-1.0433	0.226	0.57
±	0.3242		0.364	0.433	0.2733			0.395		
lnDU	5.2962			-2.3538			-5.1786		0.557	0.53
±	1.6004			0.7793			0.8921			
lnDNb	-22.27	2.3241		3.7633	2.9786	1.44	1.8719		0.446	0.6
±	3.8207	0.4364		0.8944	0.5331	0.1552	0.751			
lnDZr	-25.6167	2.6183	2.6867	4.838	2.6591	0.6536	2.5248		0.489	0.46
±	6.2797	0.646	0.8747	1.4983	0.7124	0.1496	0.927			
lnDLa	-20.0493	2.0732		2.5498	1.5317	1.117	2.2771	-1.4576	0.338	0.69
±	2.7427	0.3151		0.6107	0.2794	0.1325	0.5098	0.4684		
lnDCe	-21.1078	2.4749		2.4719	1.5722	0.952	1.5311		0.316	0.82
±	2.747	0.3122		0.7001	0.2899	0.1451	0.4978			
lnDNd	-20.3082	2.5162		2.5863	1.9459	0.9566	1.2763		0.362	0.71
±	2.869	0.3125		0.7628	0.2911	0.1264	0.5252			
lnDSm	-11.3625	1.602			1.2898	1.2376			0.426	0.6
±	0.614	0.1046			0.29	0.1218				
lnDEu	-35.6604	4.1452	2.6886	6.4057	3.8508	0.7255	3.0679		0.372	0.77
±	7.2875	0.7354	1.0276	1.6219	0.7596	0.1546	1.1127			
lnDGd	-19.0583	2.4417		1.9786	1.8765	0.9943	1.3677		0.403	0.66
±	3.5099	0.3715		0.8105	0.3785	0.1607	0.6517			
lnDDy	-16.0687	2.3858		1.8255	1.9741	0.6922			0.333	0.79
±	1.1469	0.1721		0.4663	0.2559	0.1077				
lnDHo	-20.4148	2.3654		2.484	3.2601	1.2922	3.1762	-4.9224	0.398	0.84
±	4.9365	0.5324		1.3325	0.6081	0.4288	1.1052	1.0816		
lnDYb	-15.8659	2.281		1.5905	2.1534	0.7867			0.426	0.66
±	1.4239	0.2228		0.5474	0.3275	0.1684				
lnDLu	-19.3462	2.1142		2.8478	2.7011	1.0402	2.9625	-3.2356	0.395	0.74
±	3.3662	0.3998		0.8937	0.6972	0.2336	0.9835	0.876		
lnDY	-36.2514	3.6078	3.78	7.513	4.8366	0.814	4.6048		0.323	0.71
±	7.9576	0.9806	1.0445	1.6764	0.7101	0.1737	0.7871			

e.g. $\ln D_{La} = -20.0493 + 2.0732*Si + 2.5498*Ti + 1.5317*Fe^{3+} + 1.117*Fe^{2+} + 2.2771*Ca - 1.4576*Na_A$

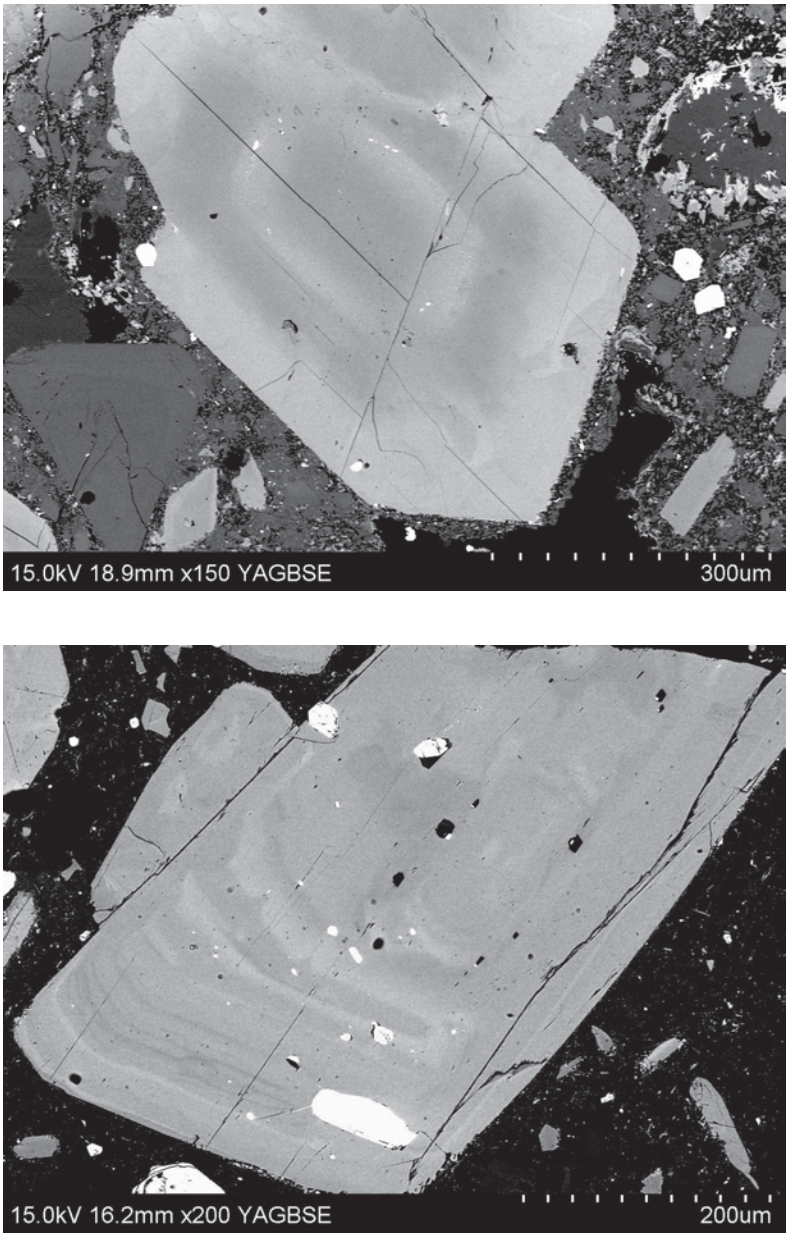

Supplementary figure S1.
Representative back-scattered electron images illustrating “diffuse-zoned” (top, from LAM-14) and “spiky-zoned” (bottom, from LAM-23) oscillatory zoning, showing multiple excursions to high Mg-number.